Electronic Supplementary Information:

Manipulating the Dynamics of Mechanochemical Ternary Co-Crystal Formation

H. Kulla, Adam A.L. Michalchuk and Franziska Emmerling

CONTENTS

S1. EXPERIMENTAL DETAILS

S1.1 Materials

In all cases, commercial chemicals were used: glutaric acid (Acros Organics, > 99%), isonicotinamide (Acros Organics, > 99%), pyrazinamide (Merck, for synthesis) and pyrazin-2-carboxylic acid (Merck, for synthesis). All compounds were used as obtained, without further purification.

S1.2 Mechanochemical Synthesis

Mechanochemical reactions were performed within PMMA milling vessels. These have been demonstrated to allow collection of *in situ* real time X-ray diffraction and Raman scattering.[1] For each reaction, stoichiometric quantities of material with total mass of 1 g, Table S1.1. For liquid assisted grinding experiments, 0.2 mL liquid was added to the vessel. Each reaction was driven by the addition of two milling balls (stainless steel, 4 g, diameter 10 mm).

Table S1.1: Mass quantities used in the mechanosynthesis of binary and ternary cocrystals.

	Isonicotinamide (IA)	**Glutaric acid (GA)**	**Pyrazinamide (PZA) / Pyrazine-2-carboxylic acid (POA)**
IA:GA:PZA	0.324 g	0.350 g	0.326 g
IA:GA:POA	0.323 g	0.349 g	0.328 g
IA:GA	0.480 g	0.520 g	--
GA:PZA	--	0.516 g	0.484 g
IA:POA	0.496 g	--	0.504 g

S1.3 *In situ* Analysis

All *in situ* XRD measurements were carried out on the µSpot beamline (BESYY II, Helmholtz Centre Berlin for Materials and Energy). The beam was monochromated to $\lambda = 1.000$ Å by means of a double-crystal Si (111) monochromator. A spot size of 100 µm diameter was used. Scattering was collected on a 2D MarMosaic CCD detector (3072 x 3072 pixels, pixel size 73 µm). Diffraction patterns were obtained by

accumulating scatter for periods of 30 s. This ensures averaging over the powder as it moves through the beam during milling. Subsequent diffraction patterns were separated by a delay of 3 s to ensure no overlap of signal between frames. The X-ray beam was focused so to minimise its path through the same. This allows us to minimise double reflections. The resulting 2D X-ray diffraction patterns were processed using the FIT 2D program. Diffraction patterns were background corrected within DIFFRAC.EVA (v4.2, Bruker AXS, Germany).

Raman spectra were collected using a non-contact Raman probe with excitation wavelength λ = 785 nm and a spot size of 1.0 mm. The *in situ* real-time Raman spectroscopic measurements were performed with laser power of 400 mW, and collected using a Raman RXN1 ™ Analyzer (Kaiser Optical Systems, France). Each Raman spectrum was collected by summation of 5 independent spectra, each resulting from 5 s of accumulated intensity. The mean spectral resolution was 4 cm^{-1}.

S1.4 Structure Solution from Powder-X-ray Diffraction Data

Products obtained by milling were analysed *ex situ* by powder X-ray diffraction (PXRD) using a D8 Discover Diffractometer (Bruker AXS, Germany). To do this, powders were packed in borosilicate capillaries with inner diameter 0.5 mm. Diffraction was measured in transmission mode using Cu $K_{\alpha 1}$ radiation (λ = 1.54056 Å). Scattering was collected over angle $2\theta = 5 - 60^{o}$, with step size 0.009°. At each step, scattering was collected for 30 s, resulting in a total measurement time of *ca* 52 h.

Data were indexed using the programme TOPAS (v. 5) and the DICVOL algorithm, as implemented in DASH (v3.3.5). For the structure solution, suitable starting conformations for each reactant molecule were taken from the CSD. These were used as ansatz for simulated annealing, as implemented in DASH (v3.3.5). The obtained structures were Rietveld refined to validate the model, using TOPAS (v5).

S1.5 Computational Methods

Each of the newly solved crystal structures were minimised by plane wave Density Functional Theory (pwDFT) calculations, as implemented in QuantumESPRESSO v6.4.[3] The electronic structure was expanded in plane waves to a maximum kinetic energy of 60 Ry, and sampled on a Monkhorst-Pack[4] grid of spacing < 0.05 A^{-1}. The exchange-correlation function of Perdew-Burke-Ernzerhof (PBE)[5] was used with Grimme's D3 dispersion correction, including the C9 correction.[6] Ultrasoft pseudopotentials were used throughout. Only atomic positions were relaxed, and the experimentally determined lattice parameters held constant. Atomic positions were accepted with residual forces < 4E-4 Ry/A and SCF convergence < 1E-8 Ry.

The isolated glutaric acid molecule was extracted from the optimised TCCs. The molecules were optimised using ORCA v4.1[7] in the gas phase using B3LYP/cc-pVDZ.[8,9] The fully optimised structures were subject to frequency calculation and found to correspond to minima on the potential energy surface. The internal energy difference of the molecules was compared.

S2. CRYSTALLOGRAPHIC STRUCTURES OF TERNARY COCRYSTALS

S2.1 Pyrazinamide : Isonicotinamide : Glutaric Acid

The crystal structure of the ternary pyrazinamide: glutaric acid: isonicotinamide (1: 1: 1) cocrystal was solved from powder X-ray diffraction data. To validate the stability of the proposed structure, the experimentally determined structure was submitted to relaxation by pwDFT methods. The resulting atomic positions are in good agreement with those obtained experimentally, suggesting they are present in stable conformations. A total correlation of RMSD of < 2% was found, Figure S2.1.

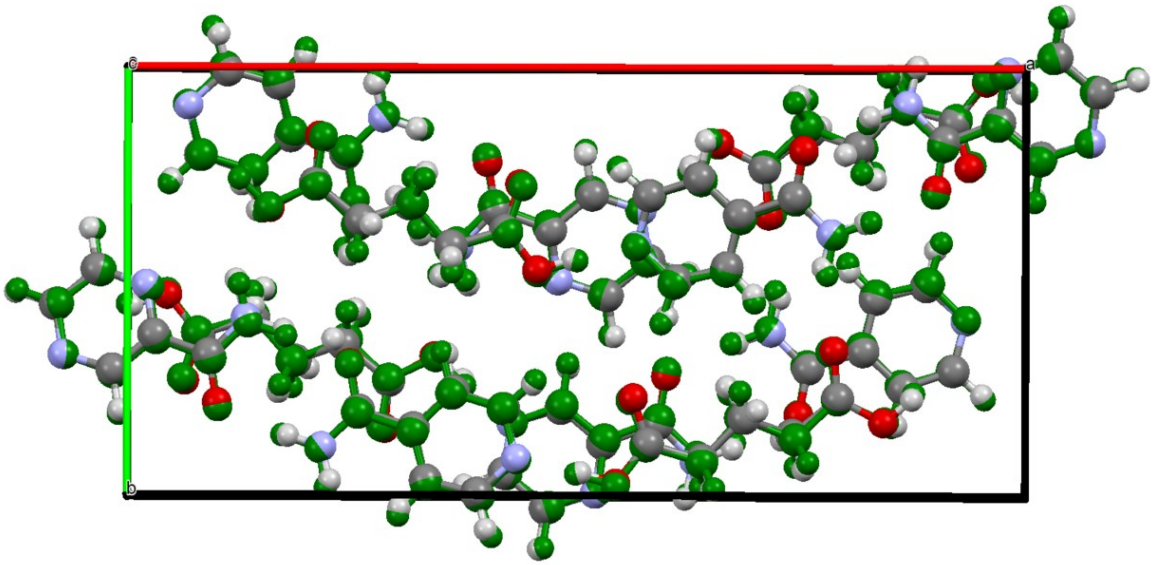

Fig. S2.1: Overlay of unit cell structure for PZA:IA:GA TCC. The (green) DFT optimised structure agrees well with the (coloured) experimentally determined atomic positions.

The DFT-optimised structure was subsequently refined against the experimental data by Rietveld method, using restraints on bonds and angles. The overlay of DFT and DFT+refined atomic coordinates is given in Figure S2.2 with RMSD < 1%. The corresponding Rietveld refinement is given in Figure S2.3. The associated crystallographic data is given in Table S2.1

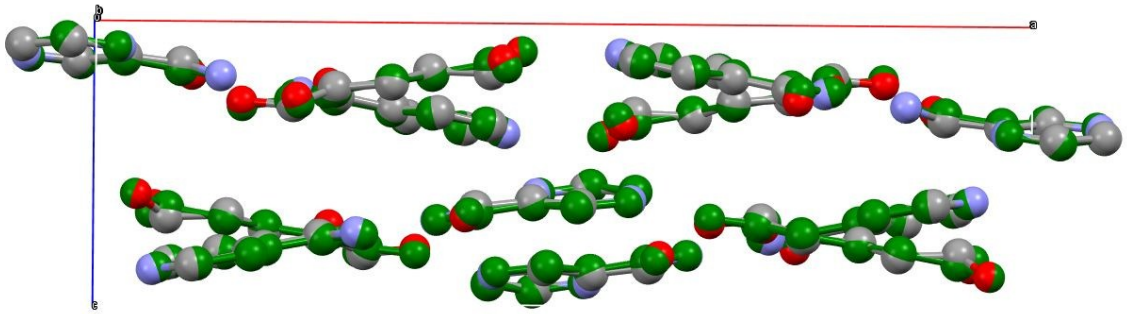

Figure S2.2: Overlay of unit cell structure for PZA:IA:GA TCC. The (green) DFT optimised structure agrees well with the atom refined structure (coloured) obtained from Rietveld refinement of the XRPD data.

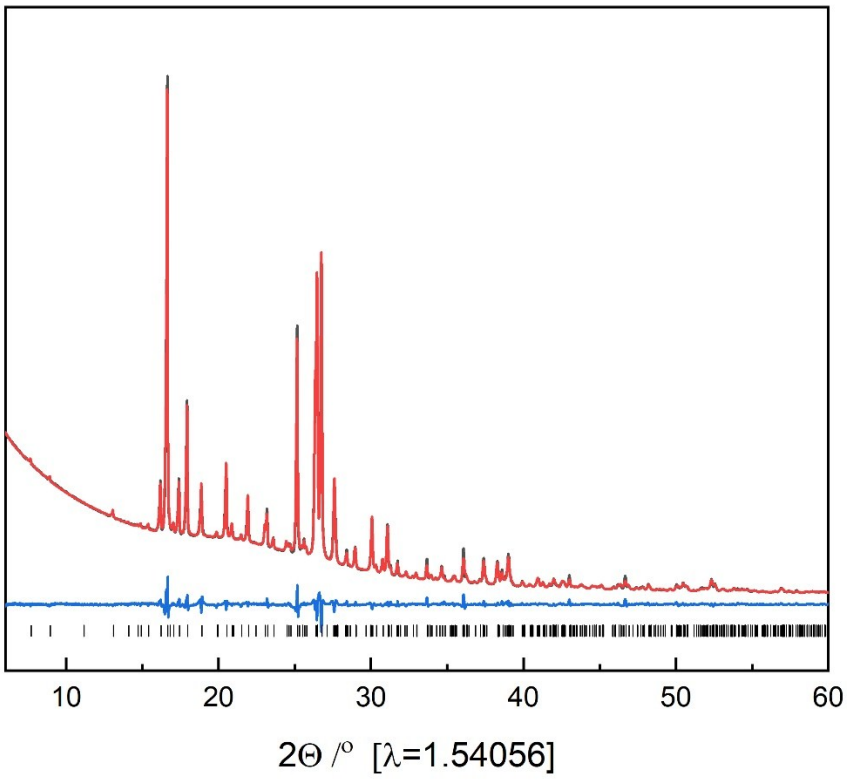

Figure S2.3: Rietveld refinement of DFT simulated, and subsequently atom refined PZA:IA:GA TCC against experimental data. (Red) simulated pattern; (black) experimental pattern; (black ticks) Bragg reflections; and (blue curve) difference curve. Background has been subtracted.

Table S2.1: Crystallographic data for ternary cocrystal pyrazinamide (PZA) : glutaric acid (GA): isonicotinamide (IA) at *ca* 293 K. Data corresponds to DFT+Rietveld refined structure.

	PZA:GA:IA 1:1:1
Chemical composition	$(C_5H_5N_3O) \cdot (C_5H_8O_4) \cdot (C_6H_6N_2O)$
Molar mass [g·mol^{-1}]	377.35
Crystal system	Orthorhombic
Space group	$P2_12_12_1$
a [Å]	22.9747(7)
b [Å]	10.9249(3)
c [Å]	7.06559(18)
α [°]	90
β [°]	90
γ [°]	90
Z	4
V [Å^3]	1773.44(8)
R_{wp}	2.643
R_{Bragg}	1.464
GOF	5.27

The PZA: GA: IA cocrystal crystallizes in the orthorhombic space group $P2_12_12_1$. The primitive unit cell contains 4 units of each molecule. The cocrystal consists of infinite chains that form a network through intermolecular N-H · O hydrogen bonds, Figure S2.4. This results in layers that are arranged parallel to each other, with every second chain being in the same plane.

Within each chain, glutaric acid forms hydrogen bonds with the aromatic nitrogen atoms of isonicotinamide (d(D · A) = 2.626 Å) and pyrazine amide (d(D · A) = 2.694 Å) *via* O H · N interactions. In addition, the amides form an R22(8) heterosynthon *via* N-H O (d(D · A) = 2.965 Å and 2.909 Å) interactions. The hydrogen atoms of the amide groups that are not involved in this are responsible for the cross-linking to glutaric acid units of adjacent chains *via* N-H ··· O hydrogen bonds with d(D·· A = 2.989 Å) for isonicotinamide and d(D · A) = 2.939 Å for the pyrazine amide.

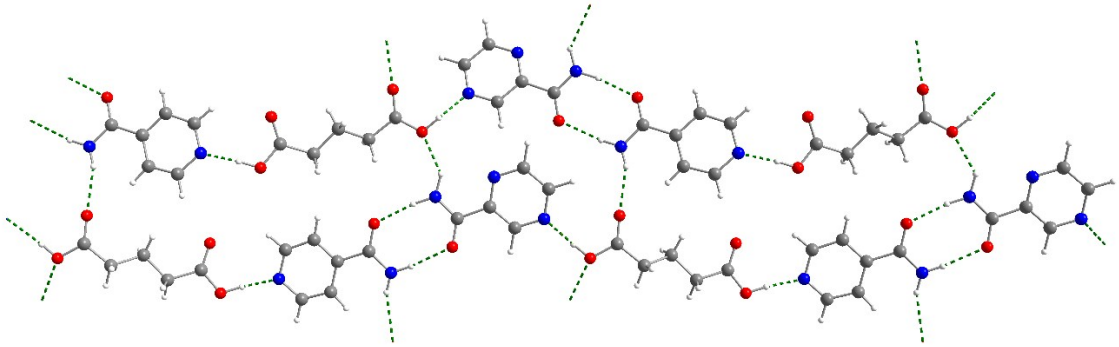

Figure S2.4: Hydrogen bonded chains within the PZA:GA:IA ternary cocrystal. Putative hydrogen bonds are represented with dotted lines. Atoms are coloured as (white) hydrogen, (grey) carbon, (blue) nitrogen and (red) oxygen.

S2.2 Pyrazine Carboxylic Acid : Isonicotinamide : Glutaric Acid

The crystal structure of pyrazine-2-carboxylic acid: glutaric acid: isonicotinamide (1: 1: 1) Cocrystal was solved from powder X-ray diffraction data. To validate the stability of the proposed structure, the experimentally determined structure was relaxation by pwDFT methods. The resulting atomic positions are in good agreement with those obtained experimentally, suggesting they are present in stable conformations. A total correlation of RMSD of < 2% was found, Figure S2.5.

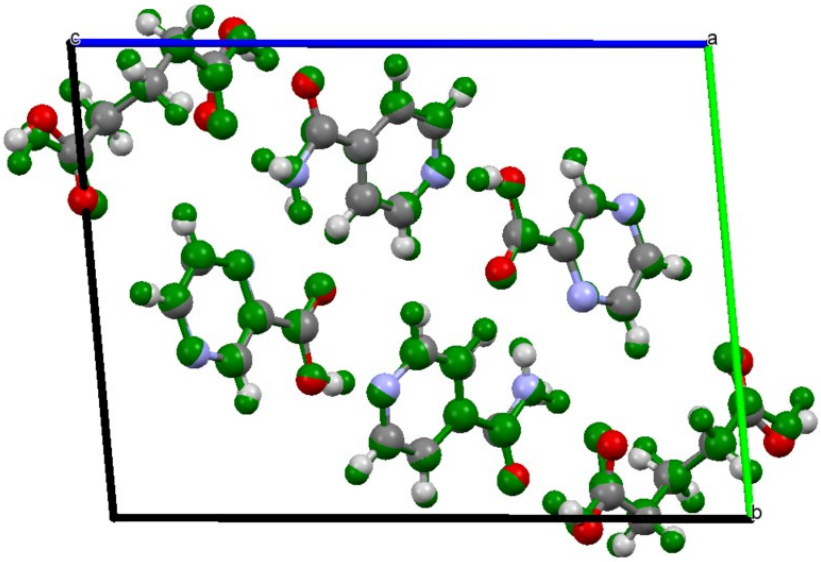

Fig. S2.5: Overlay of unit cell structure for POA:IA:GA TCC. The (green) DFT optimised structure agrees well with the (coloured) experimentally determined atomic positions.

The minor adjustments in atomic positions which result upon DFT optimisation lead to minor changes in the simulated Bragg reflections, particularly at low angle. These greatly improve the fit to the experimentally observed diffraction pattern, particularly after Rietveld refinement of the DFT-optimised structure (with bond angle and bond length restraints), Figure S2.6. We note that, as the powders were generated mechanochemically, the powder quality is adversely affected. Slight discrepancies in peak intensities and peak shape can therefore be expected. The resulting crystallographic data are given in Table S2.2

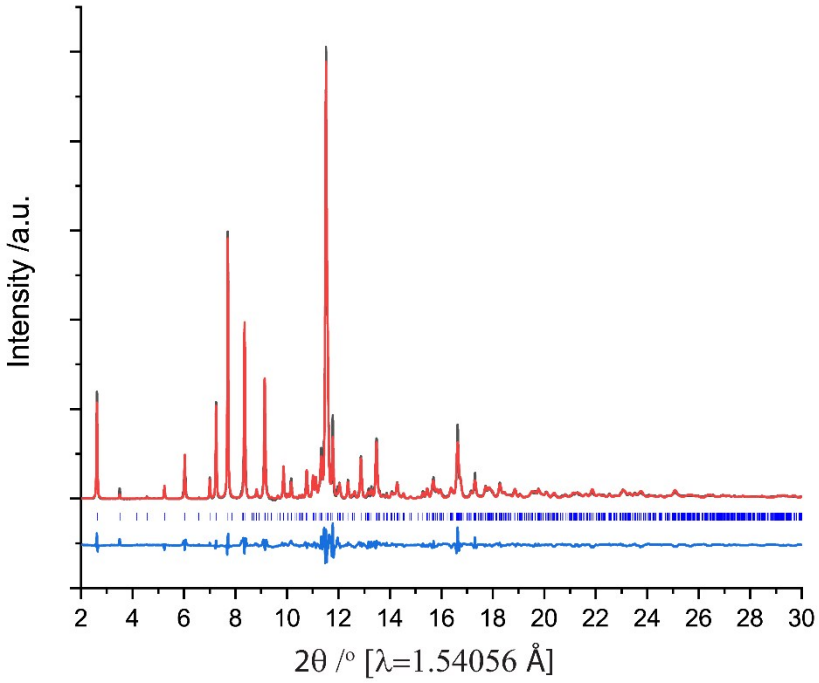

Figure S2.6: Rietveld refinement of DFT simulated POA:IA:GA TCC against experimental data. (Red) simulated pattern; (black) experimental pattern, (blue ticks) simulated Bragg peak positions; (blue curve) difference curve. Background has been subtracted.

Table S2.2: Crystallographic data for ternary cocrystal pyrazine-2-carboxylic acid (POA) : glutaric acid (GA): isonicotinamide (IA) at *ca* 293 K. Data correspond tot he structure obtained by DFT+Rietveld refinement.

	POA:GA:IA (1:1:1)
Chemical Composition	$(C_5H_4N_2O_2) \cdot (C_5H_8O_4) \cdot (C_6H_6N_2O)$
Molar mass [g·mol^{-1}]	378.33
Crystal system	Triclinic
Space group	$P\bar{1}$
a [Å]	4.91505(14)
b [Å]	11.66385(19)
c [Å]	15.5627(5)
α [°]	95.2473(11)
β [°]	90.6137(15)
γ [°]	92.843(2)
Z	2
V [Å^3]	887.25(4)
R_{wp}	3.827
R_{Bragg}	2.302
GOF	1.458

The POA: GA: IA cocrystal crystallizes in the triclinic space group $P\bar{1}$. The cocrystal consists of infinite double chains stabilized by intermolecular N-H · O hydrogen bonds (d(D · A) = 2.940 Å), Figure S2.7.

The layers formed by these hydrogen bonding interactions run parallel to an identical double-chain layer. Within each chain, glutaric acid forms an R22(8) heterosynthon with the amide group of isonicotinamide *via* NH · O (d(D · A) = 3.035 Å) and OH · O (d(D · A) = 2.640 Å) interactions. The second carboxyl group of glutaric acid forms hydrogen bonds with the meta-nitrogen atom of POA (O-H ··· N, d(D · A) = 3.033 Å), thus linking the two aromatics. The chain is complemented by O-H · N hydrogen bonds between the carboxyl group of POA and the aromatic nitrogen of isonicotinamide (d(D · A) = 2.575 Å). The primitive unit cell contains two units of each molecule, Figure S2.7.

.

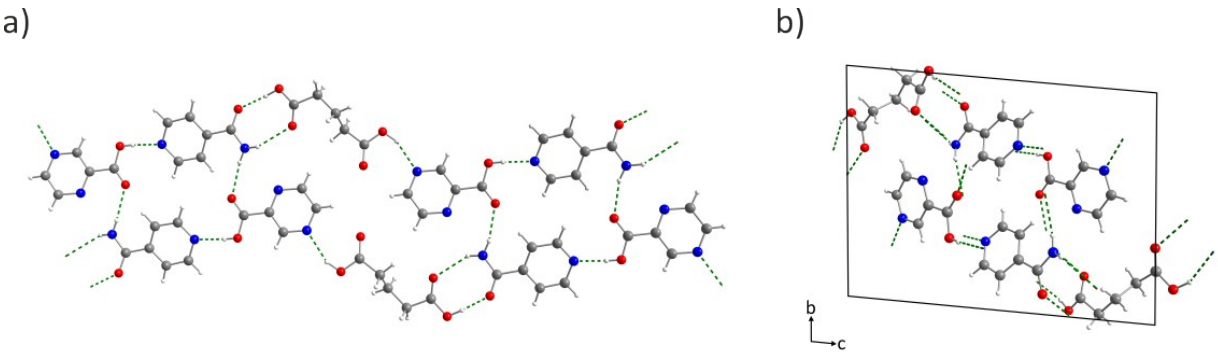

Figure S2.7: Crystal structure of POA:IA:GA ternary cocrystal. (a) Structural motif and (b) Crystal structure . Putative hydrogen bonds are represented with dotted lines. Atoms are coloured as (white) hydrogen, (grey) carbon, (blue) nitrogen and (red) oxygen.

S2.3 Glutaric Acid Conformation

The glutaric acid ion was extracted from the optimised unit cell and relaxed in the gas phase. It was compared to the optimised glutaric acid ion, as found in the orthorhombic structure (PZA:IA:GA), Figure S2.8. The absolute energy difference shows that the glutaric acid conformation found in POA:IA:GA is only *ca* 2.8 KJ/mol higher in energy than that of PZA:IA:GA. This is on the same order of magnitude as the thermal energy contained within the system (RT $\approx$ 340 K). The difference in energy can be expected to be lower within the solution phase.

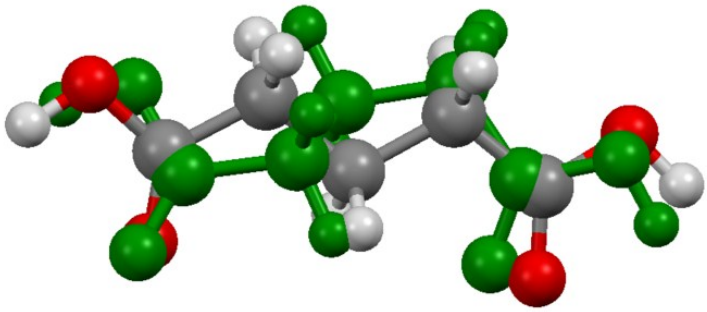

Figure 2.8: Comparison of the optimised gas phase geometries of glutaric acid molecules in the two TCCs. That optimised from the PZA:IA:GA structure is given in colour, and that from POA:IA:GA in green. The absolute energies from B3LYP/cc-pVDZ are PZA:IA:GA (-496.054751605362 Ha) vs POA:IA:GA (-496.055832695599).

S3. MECHANOCHEMISTRY OF PZA : GA : IA

S3.1 Mechanochemical formation of GA : IA and PZA : GA

To observe whether the PZA : GA binary cocrystal could form under neat mechanochemical conditions, the stoichiometric mixture of the two components were milled at 50 Hz and monitored by X-ray diffraction, Figure S3.1. Within approximately 15 minutes of milling, the entire reaction mixture was found to convert to the binary phase. A stoichiometric mixture of IA + GA was also milled for 60 mins at 50 Hz, and resulted in transformation to the corresponding binary cocrystals, Figure S3.2. Hence, it is plausible to expect also formation of this binary phase within the three-component mixture, as discussed in the main text.

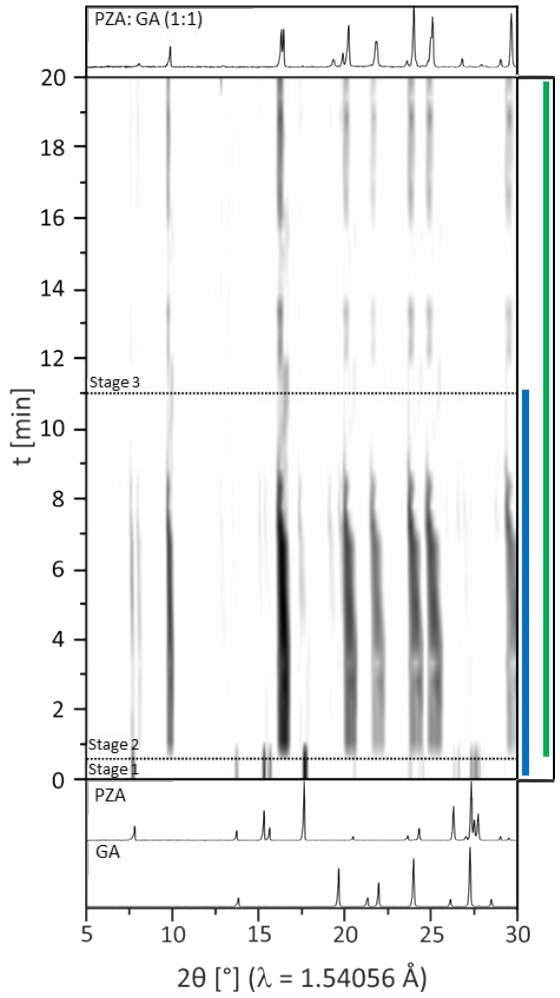

Figure S3.1. Time resolved powder X-ray diffraction for the mechanochemical synthesis of PZA:GA from stoichiometric starting components. Milling at 50 Hz. Colours indicate presence of (blue) reactants and (green) product phases.

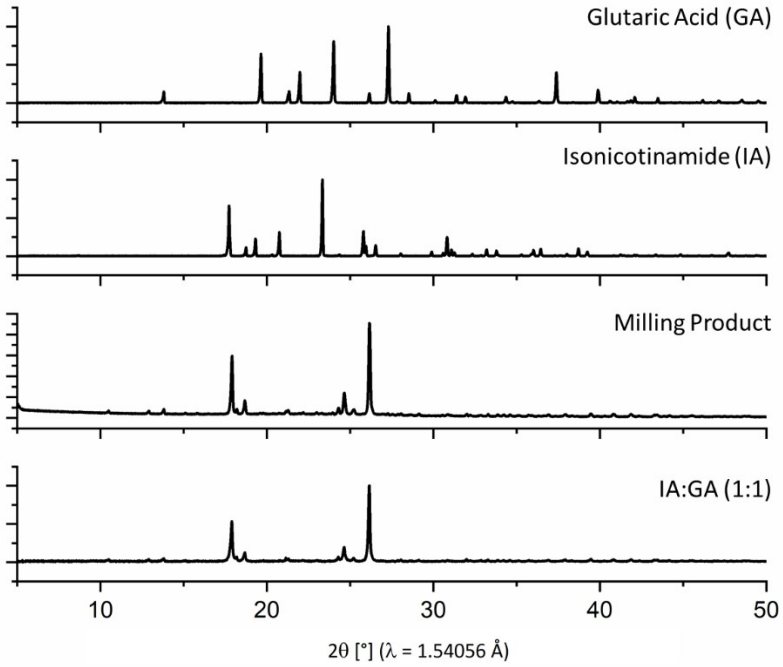

Figure S3.2: Milling of 1:1 mixture of IA + GA at 50 Hz for 60 mins. Comparison of experimental diffraction profile suggests complete conversion to the binary co-crystal phase, IA:GA.

S3.2 Milling binary cocrystals + third component

The data discussed in Figure 1 (main text) describes the mechano-synthesis of ternary cocrystal PZA:GA:IA from a mechanical mixture of the three reactant phases. When grinding at 50 Hz, the ternary phase was also found to form by cogrinding either of the known binary phases (IA:GA or PZA:GA) with the third component, Figure S3.3. In the case of grinding PZA:GA + IA, the ternary phase is formed very rapidly, with initial product reflections observed after only *ca* 45 – 60 s (stage 2). The conversion of binary PZA:GA to the ternary phase is complete after *ca* 120 s. Continued grinding of the ternary cocrystal does not lead to any further changes in the diffraction pattern (stage 3).

Cogrinding IA:GA + PZA is somewhat more complicated. After approximately 120 s grinding, two reflections at $2\theta = 19.7° \; and \; 22.3$ appear (blue ovals in Figure S3.3b). These do not correspond to any known phase of the starting components or binary cocrystal. We suppose this is indicative of a new polymorphic phase, although further testing is required. The ternary cocrystal forms after *ca* 3.5 min grinding (stage 2), and is complete by 10 min (stage 3). This unknown intermediate phase is short lived (*ca* 4 min), and disappears by 6 min grinding. Hence, the final product is the pure ternary cocrystal.

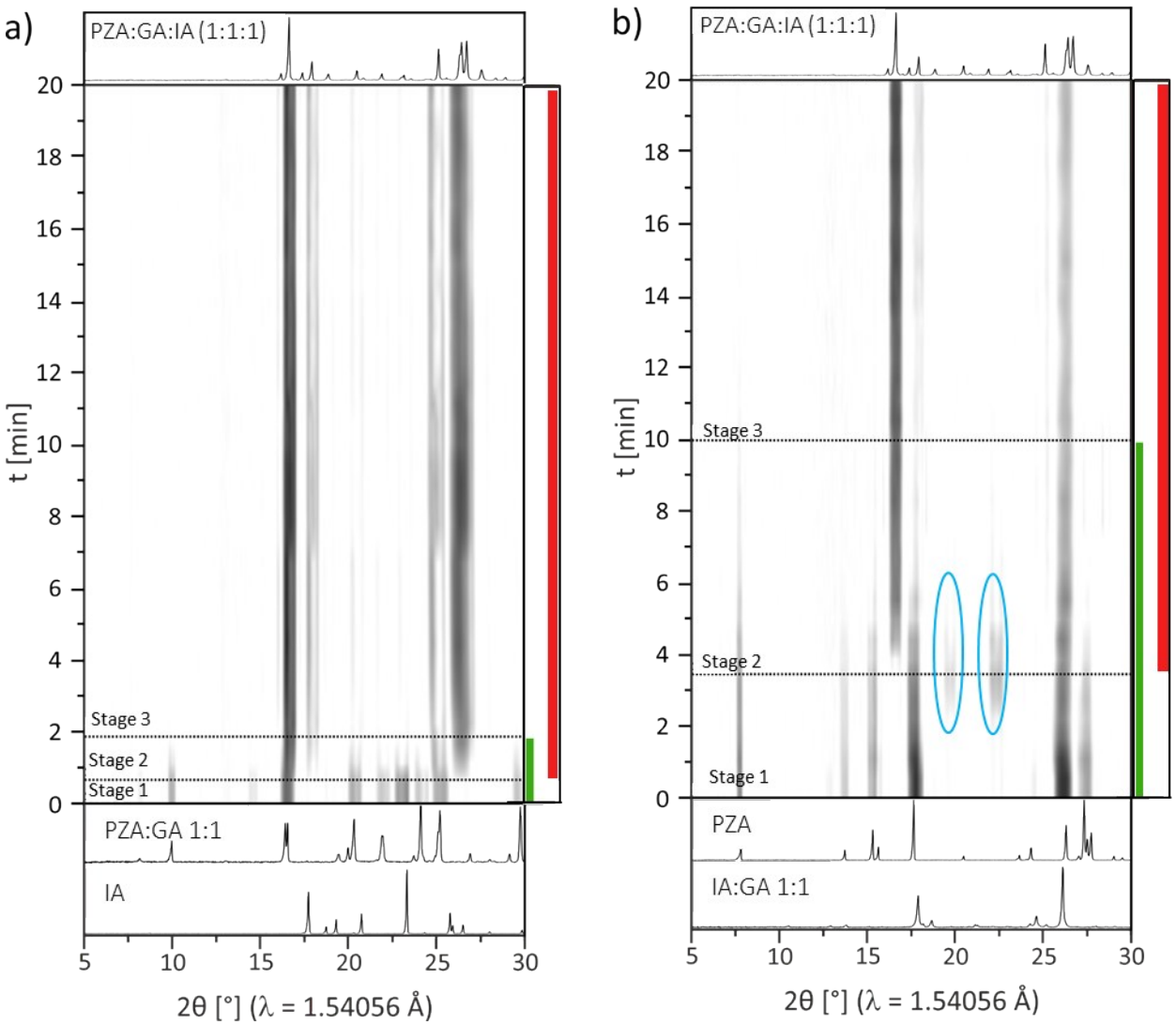

Figure S3.3. *In situ* real-time X-ray diffraction patterns for the mechanochemical formation of ternary cocrystal PZA:GA:IA. Grinding performed at 50 Hz. (a) co-grinding of binary PZA:GA + IA, and (b) co-grinding of binary IA:GA + PZA. Unknown Bragg reflections are highlighted in blue ovals. The experimental XRPD profiles for the corresponding phases are shown above and below the time-resolved data. The evolution of the binary (green) and ternary cocrystal (red) are shown schematically at the side of each plot.

S3.3. Extended Milling, TCC Stability

To assess the stability of the POA:IA:GA TCC, a stoichiometric mixture of the starting components were milled together at 50 Hz for 1 hr. The material was analysed by *ex situ* X-ray diffraction, Figure S4.4. No substantial broadening of the Bragg peaks are observed, and hence no notable loss of crystallinity is suggested to occur. The TCC is therefore stable at least up to 1 hr continuous milling.

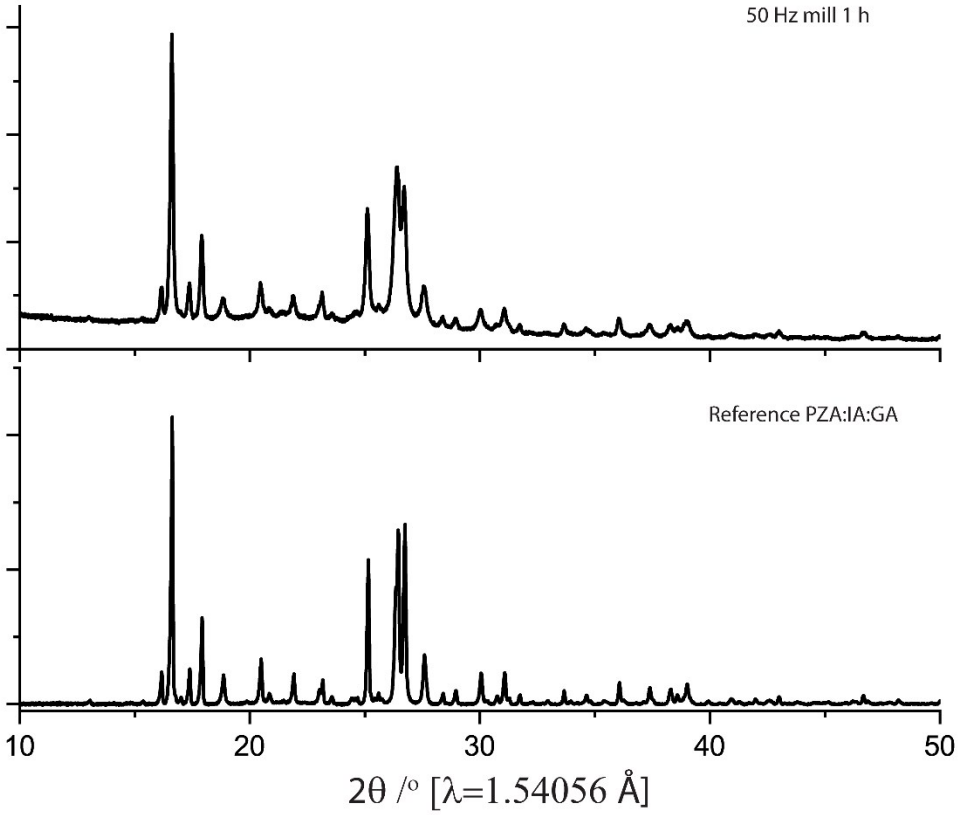

Fig S3.4: Experimental XRPD profiles obtained for mechanosynthesis of PZA:IA:GA TCC after 1 h milling at 50 Hz (Top) and the reference experimental XRPD profile for the TCC phase (Bottom).

S4. MECHANOCHEMISTRY OF POA : GA : IA

S4.1 Mechanochemical formation of POA : IA

To assess the potential of POA:IA binary cocrystals to form under neat mechanical treatment, a stoichiometric mixture of POA + IA was milled at 50 Hz for 60 min. X-ray powder diffraction of the product suggests conversion of the reaction mixture to the binary cocrystal phase, Figure S4.1. Hence, it can be assumed that this product is also accessible during milling of the ternary system, as discussed in the main text.

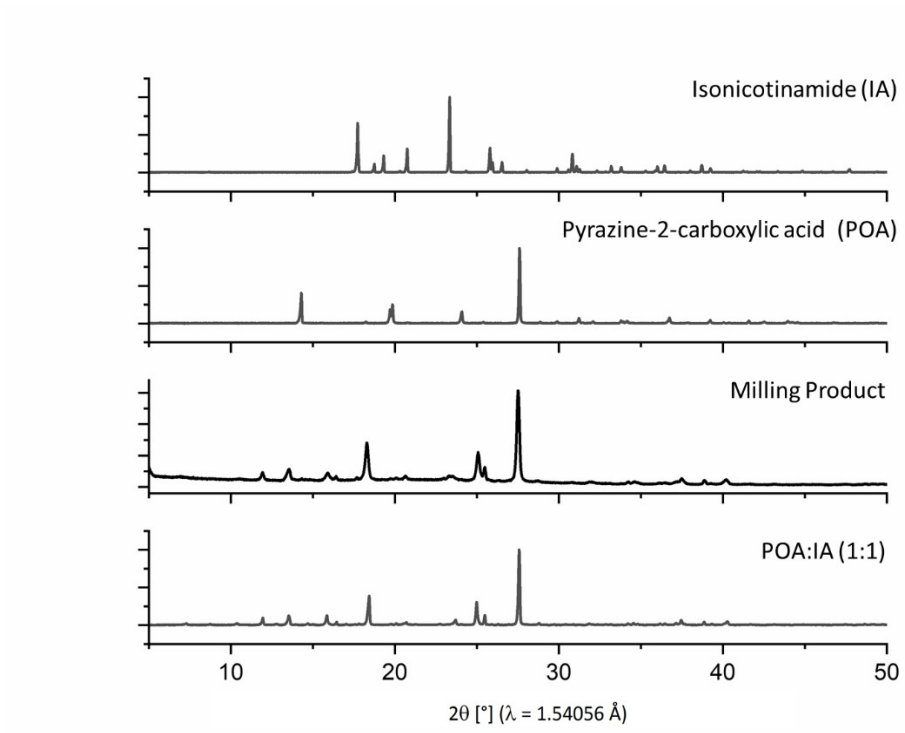

Figure S4.1: Milling of 1:1 mixture of IA + POA at 50 Hz for 60 mins. Comparison of experimental diffraction profile suggests complete conversion to the binary co-crystal phase, POA:IA.

S4.2 Milling binary cocrystals + third component

The data presented in Figure 2 (main text) describes the mechano-synthesis of ternary cocrystal POA:GA:IA from a mechanical mixture of the three reactant phases. As in Section S3, when the known binary phases (POA:GA and IA:GA) were ground at 50 Hz with the third component, the ternary phase could also be formed, Figure S4.2. In the case of grinding IA:GA + POA, the ternary phase appears to form after *ca* 5 min grinding (Stage 2), somewhat slower than the reaction of IA:GA + PZA in Figure S4.2. Furthermore, this is accompanied by a considerably longer lifetime of the unknown phase, with Bragg reflection at *ca* $2\theta = 22.3^{o}$ (blue oval in Figure S4.2A). The presence of this same phase in both reactions strongly suggests it to be due to polymorphism of the IA:GA binary phase, or of its decomposition products. The binary IA:GA converts completely to ternary PZA:IA:GA after *ca* 12 minutes of grinding, with subsequent loss of the unknown phase after *ca* 16 minutes grinding (Stage 3).

Co-grinding POA:IA + GA is comparatively fast, with onset of ternary cocrystal formation after only *ca* 1.5 min, Figure S4.2B (step 2). The conversion to the ternary phase occurs quickly, with the pure ternary cocrystal observed after *ca* 4 min grinding (step 3).

In both systems, starting from the IA:GA binary leads to considerably slower conversions to the ternary cocrystal. It is not yet known whether this stems from the relative stabilities of the binary phases, or from the fact that the IA:GA binary appears to undergo some solid-state transition upon grinding, prior to formation of the ternary product. This would thus offer an additional example of where binary phases *hinder* formation of the ternary cocrystal. This will be the subject of follow up investigation.

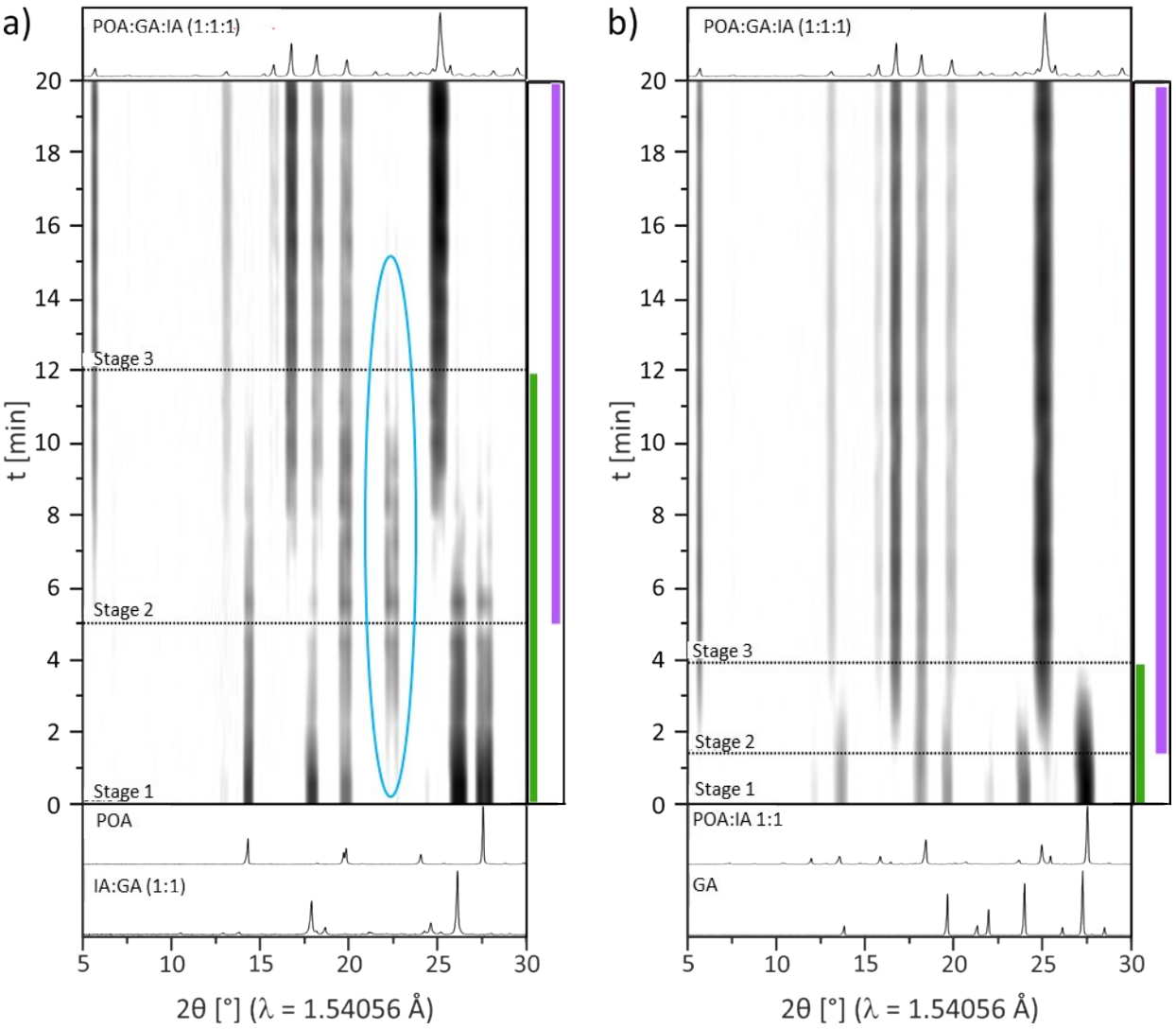

Figure S4.2. *In situ* real-time X-ray diffraction patterns for the mechanochemical formation of ternary cocrystal POA:GA:IA. Grinding performed at 50 Hz. (a) co-grinding of binary IA:GA + POA, and (b) co-grinding of binary POA:IA + GA. Unknown Bragg reflections are highlighted in blue ovals. The experimental XRPD profiles for the corresponding phases are shown above and below the time-resolved data. The evolution of the binary (green) and ternary cocrystal (purple) are shown schematically at the side of each plot.

S4.3 *In situ* Raman spectra

In addition to the *in situ* real-time PXRD analysis (Figure 2C in main text), the reaction between POA, IA and GA was monitored in real time by Raman spectroscopy, Figure S4.3. These are on the one hand the most intense Raman band of the bending vibration of the aromatic around The reaction can be followed by the vibrational bands at *ca* 1000 cm^{-1} and an additional set of bands between 1530-1630 cm^{-1}. The shifts of ν=1002 cm^{-1} to ν=1008 cm^{-1} and ν=1602 cm^{-1} to ν=1613 cm^{-1} indicate formation of the IA:GA binary phase. The ternary phase is indicated by the presence of vibrational bands at ν=1021 cm^{-1} and ν=1623 cm^{-1}. The conversion of POA to POA: GR: IA can be monitored by shift of ν=1533 cm^{-1} ν=1529 cm^{-}

[1]. In this way, the Raman spectra support the findings reported in the main text. Namely, that the neat grinding reaction proceeds directly from the initial three-component mixture into the ternary cocrystal, while the binary phase(s) form during the synthesis in the presence of solvent. In accordance with the PXRD results, when monitored by Raman spectroscopy, the reaction conducted under LAG conditions is again slower than that by neat grinding, presumably due to competitive formation of the binary phase.

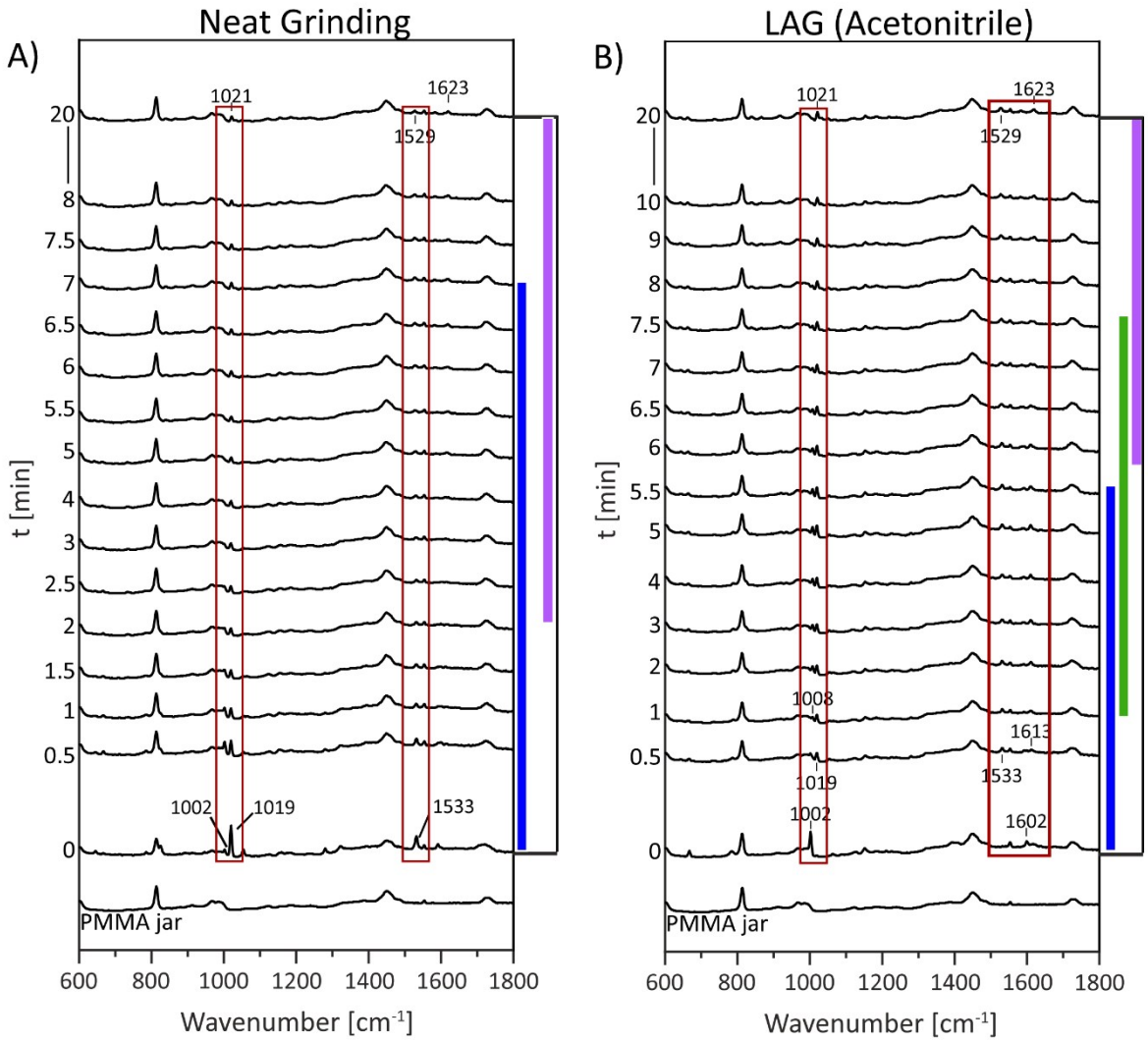

Figure S4.3: In situ real-time monitoring of mechanochemical synthesis of POA:IA:GA ternary cocrystal, monitored by Raman spectroscopy. (A) reaction monitoring under neat grinding conditions, and (B) under LAG conditions with acetonitrile used as liquid. The phase identity is indicated by colours alongside the time-resolved data as (blue) reactants, (green) binary phases and (purple) ternary cocrystal.

4.3.5 Extended Milling, TCC Stability

To assess the stability of the POA:IA:GA TCC, a stoichiometric mixture of the starting components were milled together at 50 Hz for 1 hr. The material was analysed by *ex situ* X-ray diffraction, Figure S4.4. No substantial broadening of the Bragg peaks are observed, and hence no notable loss of crystallinity is suggested to occur. The TCC is therefore stable at least up to 1 hr continuous milling.

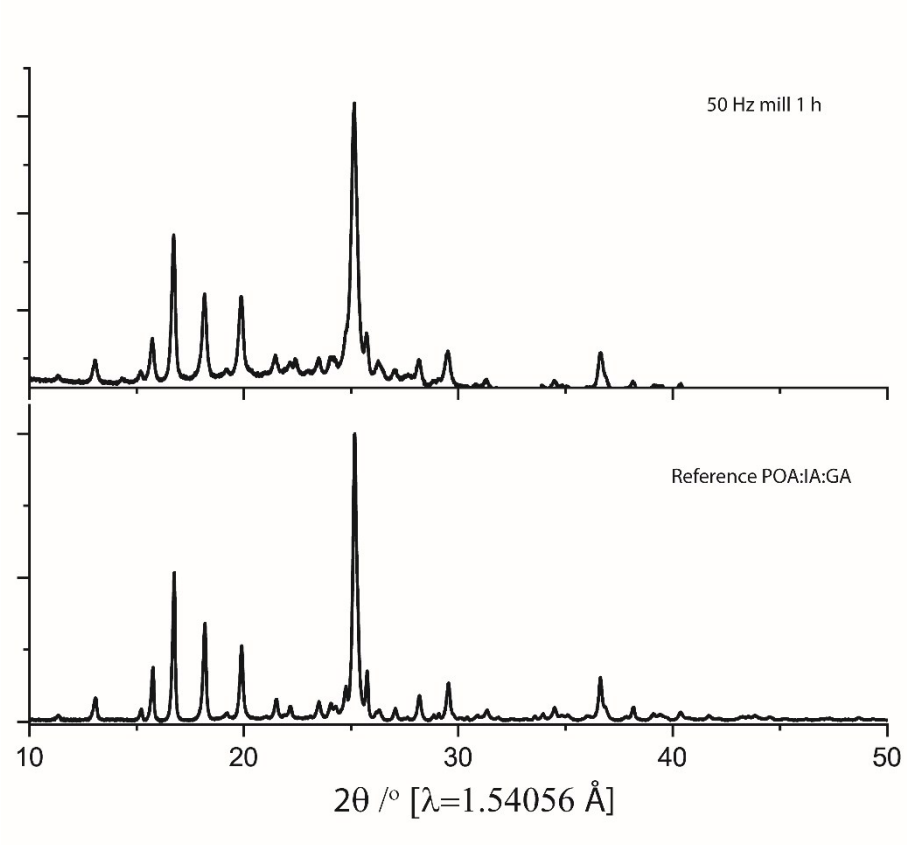

Fig S4.4: Experimental XRPD profiles obtained for mechanosynthesis of POA:IA:GA TCC after 1 h milling at 50 Hz (Top) and the reference experimental XRPD profile for the TCC phase (Bottom).

S5. ADDITIONAL *EX SITU* RAMAN SPECTRA AND DIFFRACTION DATA

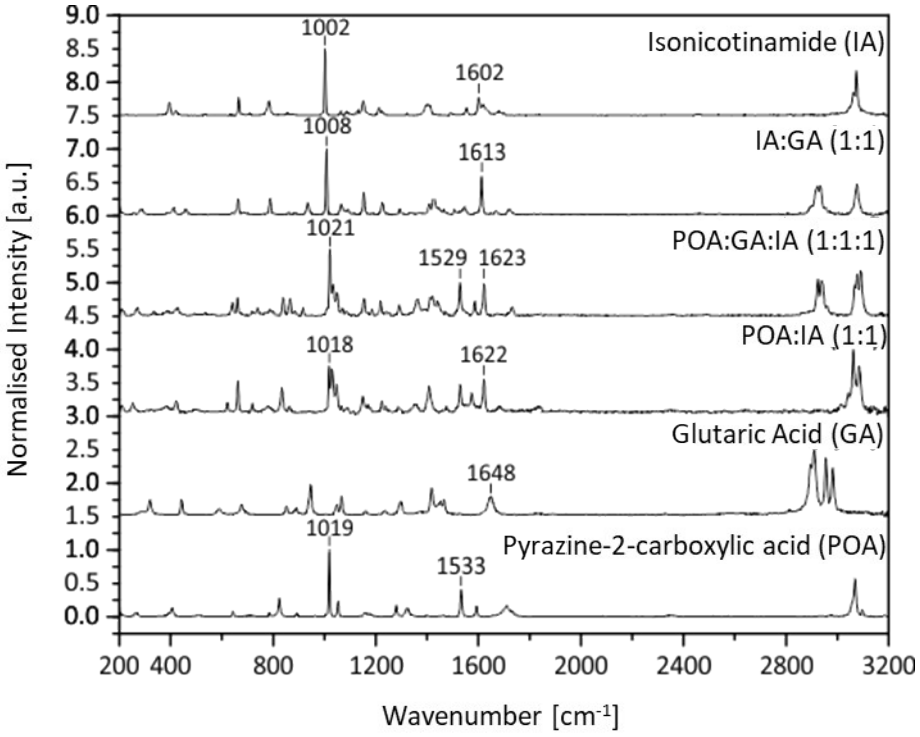

Figure S5.1: Raman spectra of the POA+IA+GA system, including pure components, binary cocrystals and ternary cocrystal phases..

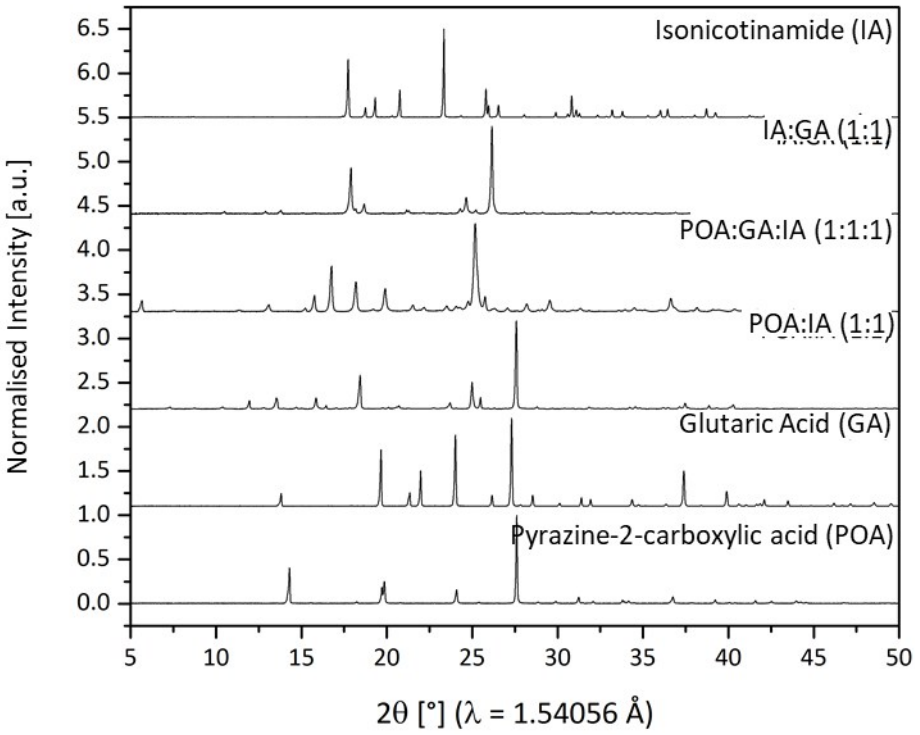

Figure S5.2: Powder X-ray diffraction data of the POA+IA+GA system, including pure components, binary cocrystals and ternary cocrystal phases.

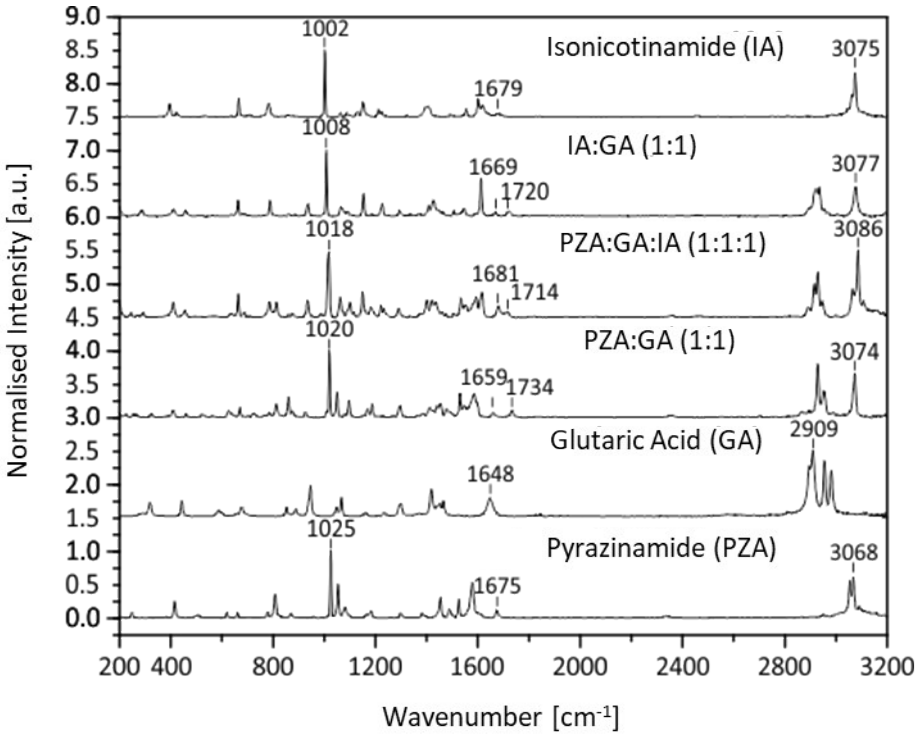

Figure S5.3: Raman spectra of the PZA+IA+GA system, including pure components, binary cocrystals and ternary cocrystal phases..

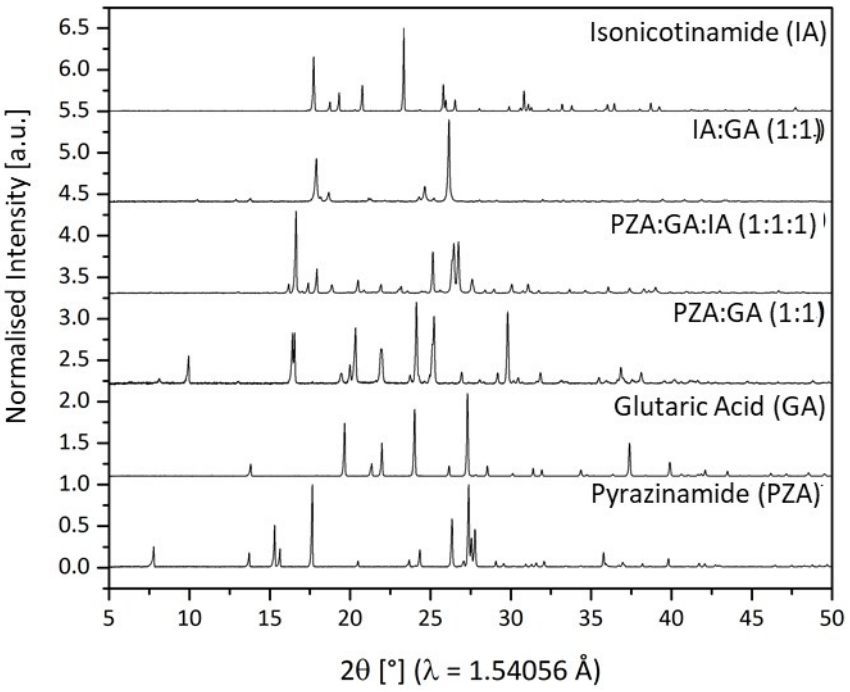

Figure S5.4: Powder X-ray diffraction data of the PZA+IA+GA system, including pure components, binary cocrystals and ternary cocrystal phases.

S6. REFERENCES

[1] L. Batzdorf, F. Fischer, M. Wilke, K.-J. Wenzel, F. Emmerling, *Angew. Chem. Int. Ed.* **2015**, *54*, 1799–1802.

[2] S. Karki, T. Friščić, W. Jones, *CrystEngComm* **2009**, *11*, 470–481.

[3] P. Giannozzi, S. Baroni, N. Bonini, M. Calandra, R. Car, C. Cavazzoni, D. Ceresoli, G. L. Chiarotti, M. Cococcioni, I. Dabo, et al., *J. Phys. Condens. Matter* **2009**, *21*, DOI 10.1088/0953-8984/21/39/395502.

[4] J. D. Pack, H. J. Monkhorst, *Phys. Rev. B* **1976**, *13*, 5188–5192.

[5] J. P. Perdew, K. Burke, M. Ernzerhof, *Phys. Rev. Lett.* **1996**, *77*, 3865–3868.

[6] S. Grimme, J. Antony, S. Ehrlich, H. Krieg, *J. Chem. Phys.* **2010**, *132*, 154104.

[7] F. Neese, *Wiley Interdiscip. Rev. Comput. Mol. Sci.* **2012**, *2*, 73–78.

[8] A. D. Becke, *J. Chem. Phys.* **1993**, *98*, 5648–5652.

[9] P. J. Stephens, F. J. Devlin, C. F. Chabalowski, M. J. Frisch, *J. Phys. Chem.* **1994**, *98*, 11623–11627.